

# Northumbria Research Link

Citation: Sandells, Melody, Löwe, Henning, Picard, Ghislain, Dumont, Marie, Essery, Richardry, Floury, Nicolas, Kontu, Anna, Lemmetyinen, Juha, Maslanka, William, Morin, Samuel, Wiesmann, Andreas and Mätzler, Christian (2022) X-Ray Tomography-Based Microstructure Representation in the Snow Microwave Radiative Transfer Model. IEEE Transactions on Geoscience and Remote Sensing. ISSN 0196-2892

Published by: IEEE

URL: <https://doi.org/10.1109/tgrs.2021.3086412>  
<<https://doi.org/10.1109/tgrs.2021.3086412>>

This version was downloaded from Northumbria Research Link:  
<http://nrl.northumbria.ac.uk/id/eprint/46240/>

Northumbria University has developed Northumbria Research Link (NRL) to enable users to access the University's research output. Copyright © and moral rights for items on NRL are retained by the individual author(s) and/or other copyright owners. Single copies of full items can be reproduced, displayed or performed, and given to third parties in any format or medium for personal research or study, educational, or not-for-profit purposes without prior permission or charge, provided the authors, title and full bibliographic details are given, as well as a hyperlink and/or URL to the original metadata page. The content must not be changed in any way. Full items must not be sold commercially in any format or medium without formal permission of the copyright holder. The full policy is available online: <http://nrl.northumbria.ac.uk/policies.html>

This document may differ from the final, published version of the research and has been made available online in accordance with publisher policies. To read and/or cite from the published version of the research, please visit the publisher's website (a subscription may be required.)



## X-ray Tomography Based Microstructure Representation in the Snow Microwave Radiative Transfer Model

|                               |   |
|-------------------------------|---|
| Journal:                      | <i>Transactions on Geoscience and Remote Sensing</i>  |
| Manuscript ID                 | TGRS-2020-02164.R2  |
| Manuscript Type:              | Regular paper   |
| Date Submitted by the Author: | n/a   |
| Complete List of Authors:     | <p>Sandells, Melody; Northumbria University, Geography and Environmental Sciences<br/>         Loewe, Henning; WSL Institute for Snow and Avalanche Research SLF, Snow Physics<br/>         Picard, Ghislain; Institut des Geosciences de l'Environnement, OSUG<br/>         Dumont, Marie; Météo-France, Centre d'étude de la Neige<br/>         Essery, Richard; University of Edinburgh Department of Geology and of Geophysics, School of Geosciences<br/>         Flourey, Nicolas; ESA / ESTEC, TEC-EEP;<br/>         Kontu, Anna; Finnish Meteorological Institute, Arctic Research<br/>         Lemmetyinen, Juha; Ilmatieteen Laitos, Space and Earth Observation Centre;<br/>         Maslanka, Will; University of Reading, Geography and Environmental Science<br/>         Morin, Samuel; Centre National de Recherches Meteorologiques Centre d'Etudes de la Neige, Centre d'Etudes de la Neige<br/>         Wiesmann, Andreas; Gamma Remote Sensing, Risk and Hazard<br/>         Mätzler, Christian; University of Bern, Institute of Applied Physics</p> |
| Keywords:                     | Electromagnetics for Remote Sensing, Cryosphere, Microwave Radiometry, Radar Data   |
|                               |   |

# X-ray Tomography Based Microstructure Representation in the Snow Microwave Radiative Transfer Model

Melody Sandells, Henning Löwe, Ghislain Picard, Marie Dumont, Richard Essery, Nicolas Floury, Anna Kontu, Juha Lemmetyinen, William Maslanka, Samuel Morin, Andreas Wiesmann and Christian Mätzler

**Abstract**—The modular Snow Microwave Radiative Transfer (SMRT) model simulates microwave scattering behaviour in snow via different selectable theories and snow microstructure representations, which is well suited to intercomparisons analyses. Here, five microstructure models were parameterized from micro-CT and thin section images of snow samples and evaluated with SMRT. Three field experiments provided observations of scattering and absorption coefficients, brightness temperature and/or backscatter with increasing complexity of snowpack. These took place in Sodankylä, Finland, and Weissfluhjoch, Switzerland.

Simulations of scattering and absorption coefficients agreed well with observations, with higher errors for snow with predominantly vertical structures. For simulation of brightness temperature, difficulty in retrieving stickiness with the Sticky Hard Sphere microstructure model resulted in relatively poor performance for two experiments, but good agreement for the third. Exponential microstructure gave generally good results, near to the best performing models for two field experiments. The Independent Sphere model gave intermediate results. New Teubner-Strey and Gaussian Random Field models demonstrated advantages of SMRT over microwave models with restricted microstructural geometry. Relative model performance are assessed by the quality of the microstructure model fit to micro-CT data and further improvements may be possible with different fitting techniques. Careful consideration of simulation stratigraphy is required in this new era of high-resolution microstructure measurement as layers thinner than the wavelength introduce artificial scattering boundaries not seen by the instrument.

**Index Terms**—snow, microstructure, microwave scattering, Snow Microwave Radiative Transfer model, SMRT

## I. INTRODUCTION

Manuscript received September 25, 2020. This work was supported in part by the European Space Agency under Grant ESTEC:4000112698/14/NL/LvH M. Sandells is with the Department of Geography and Environmental Sciences, Northumbria University, Newcastle upon Tyne, UK (e-mail: melody.sandells@northumbria.ac.uk)

H. Löwe is with the WSL Institute for Snow and Avalanche Research SLF, Davos, Switzerland

G. Picard is with IGE, Université Grenoble Alpes, Grenoble, France

M. Dumont and S. Morin are with the Université Grenoble Alpes, Université de Toulouse, Météo-France, CNRS, CNRM, Centre d'Études de la Neige, Grenoble, France

R. Essery is with the University of Edinburgh, Edinburgh, UK

N. Floury is with ESA-ESTEC, Noordwijk, The Netherlands

A. Kontu and J. Lemmetyinen are with the Finnish Meteorological Institute, Helsinki, Finland

W. Maslanka is with the University of Reading, Reading, UK

A. Wiesmann and C. Mätzler are with Gamma Remote Sensing AG, Bern, Switzerland

**S**NOW microstructure knowledge is essential to determine the scattering properties of snow at microwave frequencies. Simulations of microwave scattering are used as the basis for remote sensing of snow mass for water resources and may be used to investigate how the snow mass has changed over the last few decades. The Snow Microwave Radiative Transfer (SMRT) model has recently been developed in order to examine the impact of the representation of the microstructure, to provide a consistent theoretical treatment for passive and active simulations, and as a basis for a community model open to future developments [1]. This paper provides a thorough evaluation of the SMRT model against observations from three different field campaigns.

Many previous simulations of microwave emission and scattering in snow using inputs from in-situ measurements or snowpack evolution model simulations have a common feature: scaling of the microstructure parameters is applied in order to obtain reasonable comparison with observed radiometric data. Scaling has been applied to observations of traditional grain size [2] as used in the Helsinki University of Technology (HUT) model [3], [4], exponential correlation length [5] as used in the Microwave Emission Model of Layered Snowpacks (MEMLS) [6], [7], and sticky hard spheres [8] as used by models based on Dense Media Radiative Transfer (DMRT) theory [9]. Stickiness is a secondary (dimensionless) parameter used in the sticky hard sphere microstructure model and represents the degree of clustering between individual grains. A number of intercomparison studies between these models has illustrated different scaling factors required for each model [10], [11], [12], [13]. Stickiness itself is a challenging parameter to quantify [14].

Traditional grain size is a notoriously observer-dependent measurement and is largely incompatible with the accuracy requirements for the snow microstructure of around 0.01-0.04 mm [15]. In recent years, new instruments have been developed to measure the snow microstructure in the field from reflectivity measurements at near infrared wavelengths [16], which gives snow specific surface area (SSA) from which an optical grain diameter can be determined. Other methods of determining SSA include gas adsorption, and micro-computed X-ray tomography [17] (micro-CT). However, SSA only is insufficient to fully parameterise microstructure models. Micro-CT can provide the missing information because it gives a 3D reconstruction of the ice-air matrix from which the correlation function may be calculated and the parameters of the analytical

1 correlation functions can be fitted to the observed correlation  
2 function.

3  
4 Until recently, microwave scattering models have not kept  
5 up to date with the developments in snow microstructure  
6 observation techniques. SMRT was developed in part as a  
7 response to new instruments, especially micro-CT, but also  
8 from demonstration of the sensitivity to microstructure [15]  
9 and a need for more than one microstructure length scale.  
10 SMRT was evaluated against a substantial dataset of Arctic  
11 and sub-Arctic snow in [18] for sticky hard sphere and  
12 exponential microstructure. The present paper is the first to  
13 use tomographic microstructure observations to provide an  
14 extensive evaluation of the performance of SMRT against field  
15 observations for all SMRT microstructure models.

16 The evaluation is conducted in three steps, with data from  
17 three different field campaigns. The first step is a fundamental  
18 evaluation of the scattering and absorption coefficients given  
19 detailed microstructure information from micro-CT samples  
20 acquired during the Arctic Snow Microstructure Experiment  
21 (ASMEx) [19]. The second step is an evaluation of a shallow  
22 snowpack simulation of brightness temperature with a very  
23 simple lower boundary condition, with snowpack correlation  
24 functions given by analysis of thin section images acquired  
25 with the Passive and Active Microwave and Infrared Radiometer  
26 (PAMIR) instrument [20]. The third step is the evaluation of  
27 the active portion of the model given a snapshot of the micro-  
28 CT profile of a complete snowpack with natural substrate  
29 and to present simulations of the angular dependence of both  
30 brightness temperature and backscatter. Data are from the  
31 Nordic Snow Radar Experiment (NoSREx) [21].

32 The following section presents a brief description of SMRT.  
33 The three field campaigns and the simulation methodology  
34 are described in section III. Results are given in section IV  
35 followed by discussions and conclusions in sections V and  
36 VI.

## 37 II. SNOW MICROWAVE RADIATIVE TRANSFER MODEL

38 The Snow Microwave Radiative Transfer model [1] was  
39 developed in response to increased understanding of the im-  
40 portance of microstructure parameterisation in snow, and to  
41 enable isolation of individual model components in microwave  
42 scattering model intercomparison studies. For this, SMRT has  
43 a modular structure, which clearly separates the different steps  
44 of the calculation (permittivities of the raw materials, scat-  
45 tering coefficients, solution of the radiative transfer equation,  
46 etc.), and for each step offers different theoretical assumptions  
47 or theories that can be selected by the user. To facilitate  
48 the modular nature, SMRT is written in Python with object-  
49 oriented programming techniques and a plugin system. It has  
50 been released to the community under an open source licence  
51 (see Appendix VII on code availability) in order to allow it to  
52 be used as a general framework for future developments.

53 For evaluation of SMRT in this paper, correlation functions  
54 of the snow were determined from field samples. To focus  
55 on the microstructure model approaches, the Improved Born  
56 Approximation (IBA) was used as the electromagnetic model  
57 for all the simulations in this paper. Other theories available

in SMRT to compute scattering are specific to a particular  
microstructure form (e.g. DMRT QCA is for sticky hard sphere  
only). In IBA, the bistatic scattering coefficient (also known as  
the phase function) is defined for a 2-phase medium (subscript  
1 denotes the host constituent and subscript 2 denotes the  
scattering constituent). Radiation from the direction given  
by zenith and azimuth angles  $\vartheta', \varphi'$  is scattered into  $\vartheta, \varphi$ ,  
according to [22]:

$$p(\vartheta, \varphi, \vartheta', \varphi') = f_2(1 - f_2)(\epsilon_2 - \epsilon_1)^2 Y^2(\epsilon_1, \epsilon_2) M(|\mathbf{k}_d|) k_0^4 \sin^2 \chi \quad (1)$$

where  $f_2$  is the fractional volume of the scattering constituent,  
 $\epsilon$  is the permittivity,  $Y^2$  is the mean squared field ratio i.e. ratio  
of the field inside the scattering materials to that incident on it,  
 $M(|\mathbf{k}_d|)$  is the microstructure function,  $k_0$  is the wavevector in  
free space and  $\chi$  is the polarization angle. The microstructure  
function in IBA is determined from the Fourier Transform of the  
correlation function  $\tilde{C}(|\mathbf{k}_d|)$ , as described by [14], [1].  $\mathbf{k}_d$   
is the wavevector difference between scattering and incidence  
angles and is dependent on the effective permittivity of the  
medium computed with the Polder-Van Santen mixing formula  
[23]. For this implementation of SMRT, the simplification of  
spherical symmetry has been applied for scattering, which  
means that  $|\mathbf{k}_d|$  can be replaced with  $k_d$ . The microstructure  
function can then be calculated as:

$$M(k_d) = \frac{1}{4\pi} \frac{\tilde{C}(k_d)}{f_2(1 - f_2)} \quad (2)$$

As with any model, IBA is a theory with limitations. At  
present, only two constituents may be represented (here, ice  
and air). To allow an arbitrary arrangement of scattering  
material within the medium, the propagation speed is assumed  
constant throughout the snow layer. In this implementation the  
relationship between the electric field inside scatterers and that  
outside is assumed to be the same as for spherical scatterers  
as this ratio is more dependent on the volume fraction than  
type of scatterer [22]. Despite limitations specific to IBA, IBA  
remains closely related to DMRT theory, at least in the low-  
frequency limit [14]. DMRT was shown to be limited to small  
and moderate densities [24], [25], which is likely to apply to  
IBA, but needs further comparison with exact electromagnetic  
calculations. SMRT allows a comparison between IBA and  
DMRT at higher frequencies but is not considered in this  
paper due to the sticky hard sphere microstructure restriction  
in DMRT.

For the simulations in this paper, five different microstruc-  
ture models were used: spherical model also known as in-  
dependent sphere (IND), sticky hard sphere (SHS), exponen-  
tial (EXP), Teubner-Strey (TS) and Gaussian Random Field  
(GRF). Analytical expressions for the correlation functions in  
Fourier space as required by Equation 2 exist for all but the  
GRF model.  $\tilde{C}(k_d)$  for the SHS model, which requires sphere  
radius and stickiness as parameters, was given in equation 31  
of [14]. The microstructure functions in Fourier space for the  
IND, EXP and TS models are:

$$\tilde{C}_{IND}(k) = f_2(1 - f_2) \left( \frac{\pi d_{ind}^3}{6} \right) \left[ \frac{3(\sin X - X \cos X)}{X^3} \right]^2 \quad (3)$$

$$X = k_d d_{ind} / 2$$

$$\tilde{C}_{EXP}(k_d) = \frac{8\pi l_{ex}^3 f_2(1 - f_2)}{[1 + (k_d l_{ex})^2]^2} \quad (4)$$

$$\tilde{C}_{TS}(k_d) = \frac{8\pi \xi_{TS}^3 f_2(1 - f_2)}{[1 + Z]^2 + 2[1 - Z](k_d \xi_{TS})^2 + (k_d \xi_{TS})^4} \quad (5)$$

$$Z = \left( \frac{2\pi \xi_{TS}}{d_{TS}} \right)^2$$

where  $d_{ind}$  is the independent sphere diameter,  $l_{ex}$  is the exponential correlation length,  $\xi_{TS}$  is the Teubner-Strey correlation length and  $d_{TS}$  is the Teubner-Strey domain length (also known as repeat distance).

For Gaussian Random Field, numerical calculation of the FT of the correlation function has been applied as an analytical form cannot be found. The GRF real space correlation function (as a function of distance  $r$ ) is given as:

$$C_{GRF}(r) = f_2(1 - f_2) \frac{1}{2\pi} \int_0^{C_\psi(r)} \frac{1}{\sqrt{1 - t^2}} \exp \left[ -\frac{\beta^2}{1 + t} \right] dt \quad (6)$$

where  $\beta$  is a cut-level parameter ([26]) related to the volume fraction. The correlation function of the underlying random field currently used for the GRF in SMRT is:

$$C_\psi(r) = \exp(-r/\xi_{grf}) \left( 1 + \frac{r}{\xi_{grf}} \right) \frac{\sin(2\pi r/d_{grf})}{(2\pi r/d_{grf})} \quad (7)$$

where  $\xi_{grf}$  is the Gaussian random field correlation function and  $d_{grf}$  is the Gaussian random field domain length (or repeat distance).

The radiative transfer solver in SMRT is based on the Discrete Ordinates (DORT) approach with stream matching at the boundaries as described in [1]. Fourier decomposition is used to deal with the azimuthal dependency of the phase function and allows computation of the general solution of the radiative transfer equations by eigenanalysis, while the particular solution is obtained by solving a linear system representing the boundary conditions. So it is the Fourier Transform of the IBA phase function with respect to the azimuthal component that is used by the solver. The evaluation is done numerically.

The next section describes the three field campaigns with sufficient microstructural data to evaluate SMRT for all implemented microstructure models. Each dataset and simulation methodology are described in turn.

### III. EVALUATION DATA DESCRIPTION AND METHODS

Fitting of the microstructure models to the micro-CT data followed a common procedure for all datasets. This is described in section III-D, after the descriptions of individual field experiments.

#### A. Arctic Snow Microstructure Experiment (ASMEx)

The Arctic Snow Microstructure Experiment [19] took place in Sodankylä, Finland in the winters of 2013-2014 and 2014-2015. This field campaign was specifically designed to measure scattering and absorption coefficients of slabs of homogeneous snow in order to develop a new snow extinction coefficient model as a function of SSA for the HUT snow emission model [4], [27]. Data from this campaign included micro-CT samples and therefore provide an ideal dataset to evaluate the SMRT microstructure and electromagnetic components of the model independently from the solver. This section provides a brief description of the field measurement methodology, retrieval of scattering and absorption coefficients and simulation approach. A total of 14 horizontal snow slabs (width = 60cm, length = 80cm, various heights) were extracted and observed with microwave radiometers during the ASMEx field campaign.

Brightness temperatures ( $T_B$ )s of the snow slabs were measured on (1) a metal (highly reflecting) base and (2) microwave absorber (highly absorbing) base [27] at frequencies of 18.7, 21, 36.5, 90 and 150 GHz. A metal sheet was used to transfer the snow slab from the natural snowpack onto microwave absorbers where the metal base observations were made. The metal sheet was then carefully slid from under the snow slab to allow the snow slab to rest on the microwave absorber, as described in [19]. Measurement error specification for these instruments is 1 K, independently confirmed for 18.7-90 GHz by [21]. For ASMEx, the measurement protocol was similar in each case, with minor differences in absorber material used and frequency range observed due to equipment availability, as described in [28]. Destructive sampling of the snow slabs was then carried out roughly in order from least destructive to most destructive as described by [28]. Snow micropenetrometer profile measurements were taken first, followed by temperature, density then SSA profiles within the slab. Snow grain macro photos were also taken after SSA observations. Finally, two samples of cross-section 5 cm  $\times$  5 cm (height of slab governs the third dimension, typically around 15 cm) were taken [28], one from the radiometer centre of field of view and another in close proximity. These samples were cast in di-ethyl pththalate in the field, transported to the WSL Institute for Snow and Avalanche Research SLF in Davos, Switzerland, where they were processed and observed with an X-ray microtomography (micro-CT) instrument.

A total of 14 slabs were observed over the two winter seasons: slabs A01-A07 in the first season and slabs B01-B07 in the second. The orientation of micro-CT samples from slab A01 differed from the remaining slabs as horizontal rather than vertical profiles were taken, and only one cast sample was taken for slab A02 (for calculation of error statistics, the second A02 sample was assumed to be the same as the first). Cylindrical sections were extracted from the vertically casted snow samples and cut in half in order to fit into the micro-CT instrument, as illustrated by Figure 1. This means that a small section of snow is missing due to the thickness of the saw, although this gap is neglected for analysis purposes. Snow parameters were then determined for smaller overlapping cubic

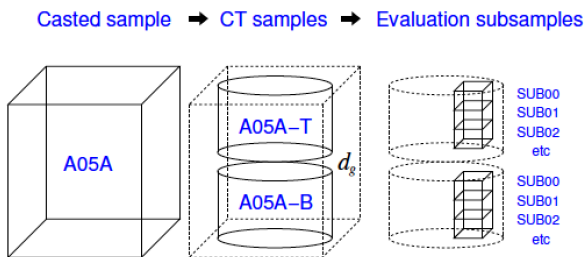


Fig. 1: Processing of slab samples (except slab A01): Slab samples were sliced into two micro-CT samples, and scanned with a nominal resolution (voxel size) of  $18 \mu\text{m}$ . Microstructure parameters were calculated over 10.8 mm stacked, overlapping subsamples

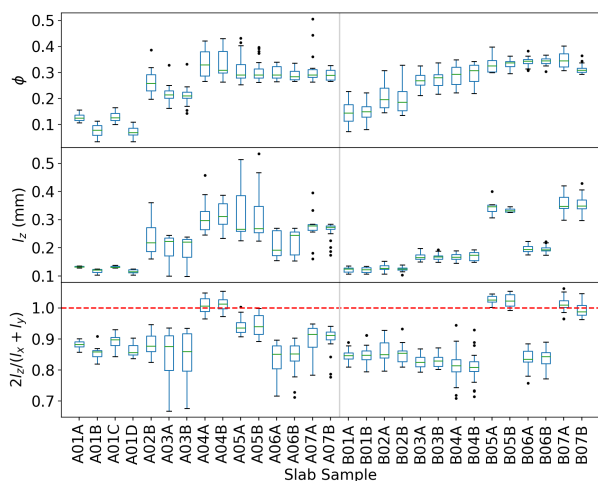


Fig. 2: Microstructure properties for 14 ASMEEx slab subsamples. Grey line separates samples taken in two different seasons. Top: fractional volume of ice; Middle: correlation length in vertical direction; Bottom: Ratio of vertical correlation length to horizontal correlation length (anisotropy)

subsamples within each micro-CT sample.

Snow density and SSA were calculated from 120 voxel height subsamples, which corresponds to a subsample height of 2.18 mm. Mean density and SSA for each of the slabs is shown in Figure 2. Although the slabs were visually homogeneous at the point of extraction, the density and SSA range within each slab shows that they are not strictly homogeneous. Early in the season (lower slab samples) the slabs are characterized by lower density and smaller microstructure scales/sizes; both generally increase as the season progresses. Perfectly isotropic snow would have equal horizontal and vertical correlation lengths i.e. anisotropy factor  $2 \ell_z / (\ell_x + \ell_y) = 1$  as shown by the red dashed line in Figure 2. An anisotropy factor of less than 1 means the correlation length is larger in the horizontal direction than the vertical, which is the case for the majority of slab samples, as expected for surface snow that has hardly undergone any temperature gradient metamorphism [29]. The microstructure is larger in the vertical for slabs

TABLE I: Summary of microstructural properties for all three experiments (IQR is interquartile range). ASMEEx and NoSREx parameters were derived from micro-CT data, PAMIR parameters were derived from thin section images. Density is given in  $\text{kg m}^{-3}$ ,  $\tau$  is dimensionless, all other microstructural parameters are given in mm. ASMEEx, PAMIR and NoSREx datasets have 562, 10 and 320 subsamples respectively.

|             | ASMEEx |      | PAMIR  |      | NoSREx |      |
|-------------|--------|------|--------|------|--------|------|
|             | Median | IQR  | Median | IQR  | Median | IQR  |
| Density     | 258    | 95   | 397    | 66   | 217    | 87   |
| $d_{SHS}$   | 0.50   | 0.38 | 0.80   | 0.38 | 0.15   | 0.16 |
| $\tau$      | 0.10   | 0.12 | 0.10   | 0.05 | 0.11   | 0.02 |
| $l_{e\pi}$  | 0.14   | 0.09 | 0.46   | 0.12 | 0.11   | 0.15 |
| $d_{JND}$   | 0.41   | 0.28 | 1.23   | 0.31 | 0.32   | 0.44 |
| $\xi_{TS}$  | 0.20   | 0.13 | 0.53   | 0.15 | 0.14   | 0.19 |
| $d_{TS}$    | 1.46   | 2.67 | 502    | 340  | 2.21   | 333  |
| $\xi_{GRD}$ | 0.14   | 0.10 | 0.37   | 0.11 | 0.10   | 0.14 |
| $d_{GRF}$   | 1.70   | 33)  | 485    | 333  | 8.12   | 334  |

A04, B05 and B07 only. Spherical symmetry is assumed in the version of SMRT used in this paper, which may not be appropriate and is discussed later in the paper.

Correlation functions of the snow were determined from the 3-D structure of the ice matrix and parameters retrieved for the five analytical correlation function models by minimisation of the cost function (further details given below). A summary of microstructure parameters for all slabs is given in Table I.

Density and microstructure parameters were used to calculate scattering and absorption coefficients for each micro-CT subsample to evaluate SMRT scattering theories independently from other SMRT modules (namely the radiative transfer solver, substrate, atmosphere and interface modules). Simulations of the absorption and scattering coefficients were carried out for all slab subsamples at all ASMEEx frequencies for all five microstructure models. Slab-means of these subsample coefficients were compared against the bulk slab coefficients retrieved from the radiometric data by [27]. As described in [27], there is a difference between coefficients retrieved from horizontally and vertically polarized observations. Here, the mean of the coefficients derived at both polarizations are used as the observations for comparison with SMRT.

For calculation of  $T_B$ , the slabs were reconstructed from the micro-CT subsamples with one snowpack layer corresponding to one micro-CT subsample with layer thickness scaled to account for mass lost during micro-CT preparation. For the simulations, the substrate was assumed to be a perfect reflector for the metal plate case, whereas for the absorber substrate, the reflectivity was determined from the measured emissivity. Where absorber emissivity observations were not available, the mean of all observations at that frequency was used. Measured downwelling atmospheric  $T_B$  was used to parameterise the simple isotropic atmosphere in SMRT (a single plane parallel layer that follows MEMLS formulation [30]) and included in simulation of  $T_B$ .

### B. Passive and Active Microwave and Infrared Radiometer (PAMIR) Snow Crust Experiment

The Passive and Active Microwave and Infrared Radiometer (PAMIR) system included five microwave radiometers at fre-

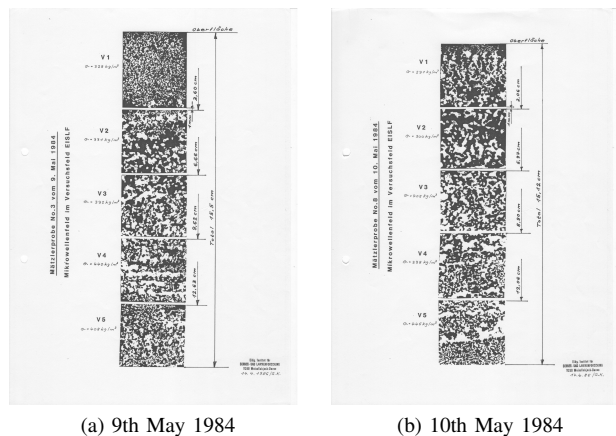


Fig. 3: Thin section images from PAMIR melt-refreeze experiment

quencies 4.9, 10.4, 21, 35 and 94 GHz (measurement error  $\sim 1$  K at 260 K [31]) mounted on a 15 m tower at an incidence angle of  $50^\circ$  at the Weissfluhjoch, Davos site from 1977 to 1987. Here, we describe a snow crust experiment that took place 8–10 May 1984 when the snowpack underwent two melt-refreeze cycles. The depth of refrozen snow was measured manually and the snowpack observed with PAMIR over the course of the experiment (33 measurements over 41 hours) [20] and two thin section images were taken, shown in Figure 3.

Correlation functions were calculated in the  $z$ - and  $x$ -direction for each of the five subsections in both images and together with the layer thickness and density observations noted in the images were used to construct a time series of snowpacks of depth given by the refrozen thickness measurements shown in Figure 4. Also shown in Figure 4 is the decrease in surface temperature and snowpack brightness temperature at 35 GHz as the snowpack refreezes, with a sudden reversal as the snowpack returns to a melting state. Table I gives a summary of the analytical microstructure model parameters derived from the thin section images, averaged over horizontal and vertical directions, where the  $y$ -direction parameters are assumed to be the same as in the  $x$ -direction.

These microstructural parameters were used to construct numerical snowpacks of time-dependent depth and assumed lower boundary emissivity of 96% at  $0^\circ\text{C}$ . Sky  $T_B$  observations were used to parameterize a simple isotropic atmosphere, which was included in the simulations. The temperatures of the snow layer midpoints were calculated by linear interpolation between the melt interface at  $0^\circ\text{C}$  and the observed temperature at the snow surface. These data were used to drive SMRT simulations and were compared to the time series of passive data from the snow crust experiment (active data were not available for comparison).

### C. Nordic Snow Radar Experiment (NoSREx)

The Nordic Snow Radar Experiment (NoSREx) took place in Sodankylä, Finland over four winter seasons and is described fully in [21]. The simulations presented here focus on

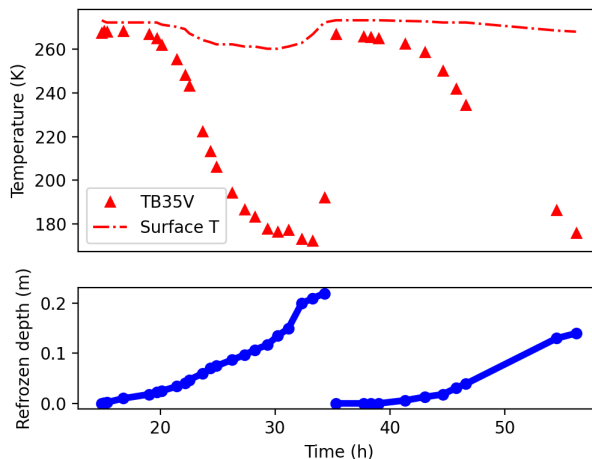


Fig. 4: Time series of refrozen snow depth (blue), surface temperature (red dot-dash line) and observed brightness temperature at 35 GHz, vertical polarization (red triangles) for the PAMIR snow crust experiment, 8-10th May 1984

the third season (2011-2012) where a near-complete micro-CT profile was available. Angular observations ( $30$ - $60^\circ$ ) of both  $T_B$  and backscatter ( $\sigma_0$ ) are available for this campaign, and thus provides the first test of SMRT in active mode. An array of radiometers (V and H 10.65, 18.7, 21, 36.5 GHz) was installed on a tower 4.1 m above ground and a four-polarization scatterometer operating between 9.2 and 17.9 GHz was mounted 9.6 m above ground nearby. As with ASME<sub>x</sub>, brightness temperature measurement error for 18.7-36.5 GHz radiometers is 1 K. Measurement error at 10.65 GHz is 2 K due to the radiometer design [21]. Backscatter measurement error is of the order 1 dB [21].

Figure 5 illustrates the non-continuous density profile determined from micro-CT data. For simulation of a continuous snowpack, layers were constructed from each available micro-CT subsample and constant layer thickness derived from the automated sensor snow depth. The temperature profile of the snowpack was estimated by linear interpolation between automated measurements of the air temperature and 2 cm below the soil surface (mean of observations at two locations) limited to a maximum of  $0^\circ\text{C}$ . A summary of the microstructural parameters over this profile is given in Table I.

For the passive simulations, soil reflectivity was calculated with [32], assuming a soil roughness root mean square height of 2 cm. The soil permittivity was determined from the mean of two soil moisture measurements at 2 cm depth, soil sand content of 70%, clay content of 1% and dry density of  $1300 \text{ kg m}^{-3}$  with the model of [33]. Atmospheric contribution was approximated with nadir observations applied to the SMRT simple isotropic atmosphere, which will result in a small underestimation in  $T_B$  as a function of incidence angle. Rather than overfitting the soil contribution in the absence of data, a soil backscatter of -13 dB was assumed to be a reasonable approximation for both HH and VV polarization. For active

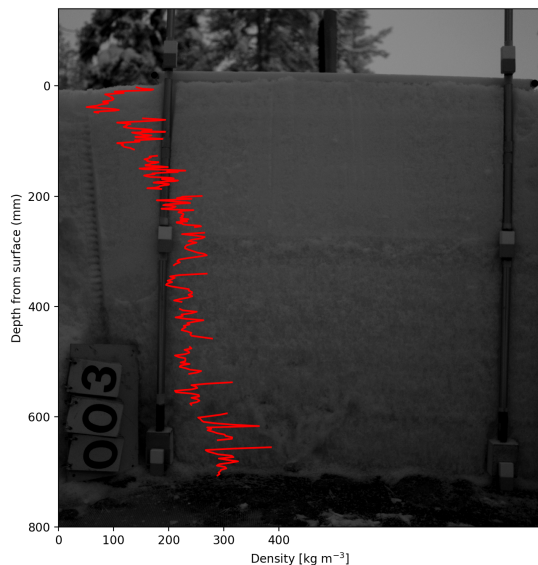


Fig. 5: NoSREx density derived from micro-CT samples overlaid on image of snowpit face. Sample taken on 1st March 2012.

simulations, micro-CT subsample layers were aggregated in groups of 20 so that the snowpack of 76 cm depth was represented by 16 layers for frequencies of 10.2, 13.3 and 16.7 GHz.

#### D. Microstructure Parameter Fitting

Similar for all data sets, the parameters for the SMRT microstructure models were obtained by fitting the autocorrelation functions obtained from binary 3D micro-CT images (NoSREx, ASMEEx) or 2D binary thin sections images (PAMIR, cf. Fig. 3a). All fits were done by using Matlab's `lsqnonlin` optimization over a fixed number of data points (100) and allowing for a global normalization prefactor. The ice volume fraction (density) was obtained directly by counting ice voxels/pixels of the images. The real space models (EXP, IND, TS, GRF) were fitted along the main coordinate directions ( $x, y, z$ ) of the 3D/2D correlation function yielding direction dependent parameters that were subsequently averaged (arithmetic mean over directions) to obtain a single set of parameters for an isotropic model. For the isotropic Fourier model (SHS) the 3D Fourier transform of the correlation function was spherically averaged and subsequently fitted.

### IV. SMRT EVALUATION RESULTS

#### A. Brightness Temperature

Brightness Temperature ( $T_B$ ) observations were available for all field campaigns. Figure 6 shows scatterplot comparisons between observed and simulated brightness temperature for each snow microstructural model and for each field campaign

TABLE II: Brightness temperature Mean Error (ME) and Root Mean Square Error (RMSE) [K]. Smallest errors for each polarization are shown in bold for each field experiment

|      |        |   | EXP         | SHS         | IND  | TS         | GRF         |
|------|--------|---|-------------|-------------|------|------------|-------------|
| ME   | ASMEEx | H | 0.5         | <b>0.2</b>  | -0.3 | -0.2       | -0.3        |
|      |        | V | <b>-3.0</b> | -3.2        | -4.0 | -3.7       | -3.9        |
|      | PAMIR  | H | 6.5         | 18.8        | 5.5  | 3.3        | <b>2.1</b>  |
|      |        | V | 7.3         | 18.9        | 6.2  | 4.0        | <b>2.8</b>  |
|      | NoSREx | H | 1.3         | 10.6        | 5.3  | <b>0.2</b> | -0.6        |
|      |        | V | 2.2         | 11.3        | 6.2  | 1.2        | <b>0.3</b>  |
| RMSE | ASMEEx | H | 22.7        | <b>22.2</b> | 25.1 | 23.3       | 23.2        |
|      |        | V | 15.3        | <b>15.0</b> | 17.5 | 15.5       | 15.4        |
|      | PAMIR  | H | 15.2        | 35.1        | 14.5 | 11.6       | <b>10.4</b> |
|      |        | V | 16.6        | 37.0        | 15.3 | 11.9       | <b>10.2</b> |
|      | NoSREx | H | 4.3         | 17.1        | 9.0  | 3.6        | <b>3.4</b>  |
|      |        | V | 3.2         | 15.1        | 7.3  | <b>3.1</b> | 3.6         |

over all available frequencies. The ASMEEx campaign observations in Figure 6a cover a wider  $T_B$  range than PAMIR and NoSREx data due to the bottom boundary condition and shallow depth of snow: low  $T_B$  observations are of slabs on top of the metal plate and high  $T_B$  were observed after the plate had been removed and the snow was on top of the microwave absorbing material. The range of  $T_B$  measured in the PAMIR and NoSREx campaigns is smaller but is more representative of observations over natural snowpacks. The microstructure model appears to have only a small influence on the simulated  $T_B$  of the ASMEEx slabs. Low  $T_B$  tend to be underestimated and high  $T_B$  overestimated for ASMEEx. Outliers in the central range of observed values (approximately 100-150 K) were slabs A02, A04 and B07 at either 21 or 36.5 GHz.  $T_B$  at other frequencies for these slabs are more closely grouped with  $T_B$  of other slabs.

PAMIR data in Figure 6b show a wide range of simulated  $T_B$  for a given observation e.g. an observed H-pol  $T_B$  of 175 K is represented by simulations over a range of 170-250 K. Simulated  $T_B$  are generally overestimated except at high  $T_B$ . However, the SHS microstructure model generally overestimates  $T_B$  by the largest amount. This is also the case for the NoSREx data in Figure 6c.

Given the more complicated structure of the full NoSREx snowpack, Figure 6c highlights the overall importance of the microstructure model, particularly at lower  $T_B$ . For the NoSREx dataset, in general the SHS model gives the highest  $T_B$ , followed by IND, EXP, TS and with GRF giving the lowest  $T_B$ . A high SHS followed by EXP, TS, GRF in decreasing  $T_B$  order is also apparent in the PAMIR dataset, although IND can be above or below EXP, or have the lowest  $T_B$  of all microstructure models. In contrast, there is no consistency between the relative  $T_B$  given by different microstructure models in the ASMEEx dataset: the order changes even for different micro-CT samples of the same slab.

Table II shows the mean error (ME) and root mean squared error (RMSE) for  $T_B$  simulated for each experiment. ME range from -4.0 to 0.5 K for ASMEEx, 2.1 to 18.9 K for PAMIR and -0.6 to 11.3 K for NoSREx. RMSE range from 15.0-25.1 K for ASMEEx, 10.2-37.0 K for PAMIR and 3.1-17.1 K for NoSREx. For the ASMEEx field campaign, RMSE are smallest for the SHS, with smallest ME for SHS (H-pol), TS (H-pol) and EXP (V-pol) microstructures. In contrast, SHS performs poorly for

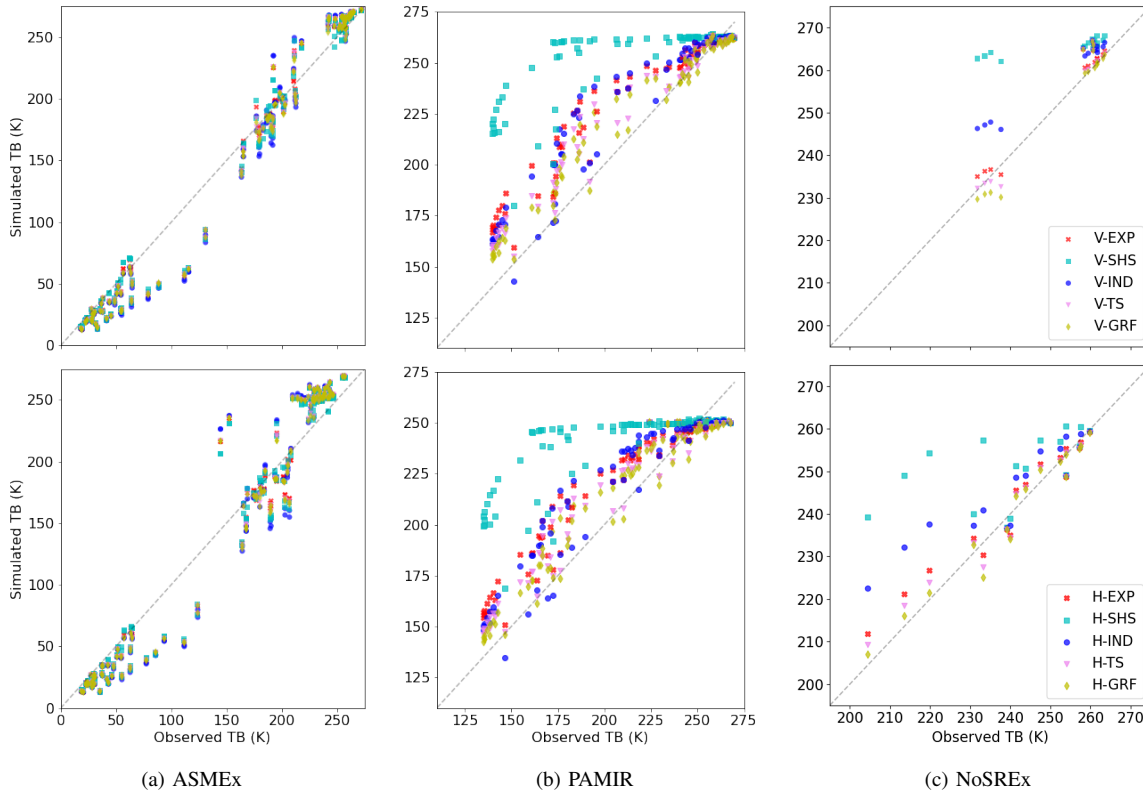


Fig. 6: Scatterplot comparison between observed and simulated brightness temperature (all frequencies observed, all incidence angles). V-polarization shown on top graphs, H-polarization shown on bottom

both PAMIR and NoSREx experiments, with largest ME and RMSE. For PAMIR and NoSREx experiments, TS and GRF microstructure models have the lowest ME and RMSE at both polarizations. The following subsections evaluate each field experiment in turn to explore these results further.

### B. Scattering and Absorption Coefficients (ASMEEx)

ASMEEx data allow evaluation of SMRT absorption and scattering coefficients against those derived in [27], as shown in Figures 7 and 8. A complete dataset is only available at 21 GHz due to instrumentation failure / installation dates at other frequencies. Calculation of the absorption coefficient ( $\kappa_a$ ) in SMRT IBA is independent of microstructure model so Figure 7 compares simulated  $\kappa_a$  (mean of subsamples) with observed  $\kappa_a$  for a single microstructure model. Note that  $\kappa_a$  in Figure 7 have been scaled by  $1/\text{wavenumber}$  to eliminate the direct frequency dependence (an indirect dependence through the permittivity remains). In general there is good overlap with the 1:1 line, with a few noticeable outliers: slabs A02, A04, B05 and B07. Slab B05 (shown by crosses) was observed at all frequencies and its  $\kappa_a$  was consistently underestimated in the simulations. At 36.5 GHz,  $\kappa_a$  for slabs A02 (downward triangle) and B07 (thin diamond) were also underestimated, although slab B07 was simulated well at 90 GHz (A02 was not measured at this frequency). At 18.7 and 21 GHz,  $\kappa_a$  for slabs A04 (leftward triangle) and B07 were also underestimated. Comparing  $\kappa_a$  with observations for all slabs, the regression

coefficient  $r^2 = 0.94$ , with root mean squared error of  $0.3 \text{ m}^{-1}$  and mean error of  $-0.2 \text{ m}^{-1}$ .

Unlike  $\kappa_a$ , scattering coefficients ( $\kappa_s$ ) depend on microstructure model, as shown in Figure 8. Note that  $\kappa_s$  have been shown on logarithmic axes. The comparison between models shows that for the ASMEEx parameters, EXP, GRF and TS models give near identical results and there is also high agreement between these models and IND. Lower regression coefficients were found between SHS and any other microstructure model, which reflect the increased scatter in SHS  $\kappa_s$ . For comparison with observations, the mean of subsample  $\kappa_s$  were compared with  $\kappa_s$  observed for the entire slab. Across all slabs,  $\kappa_s$  is generally overestimated at 90 GHz but underestimated at 36.5 GHz and below, with larger errors for lower scattering coefficients. This is not unexpected as observation errors and deficiencies in retrieval technique will have the greatest impact where least scattering occurs. It is, however, difficult to apportion the discrepancies either to the frequency-dependence of IBA or to retrieval errors. Despite these differences, observations and simulations are highly correlated. Lowest  $r^2$  between observed and simulated  $\kappa_s$  occurred for the single length scale models EXP (0.86) and IND (0.87), median  $r^2$  for SHS (0.88), and highest  $r^2$  for the TS (0.89) and GRF (0.9) models. The difference between microstructure model correlation with observations suggests choice of microstructure model influences the frequency-dependence of IBA.

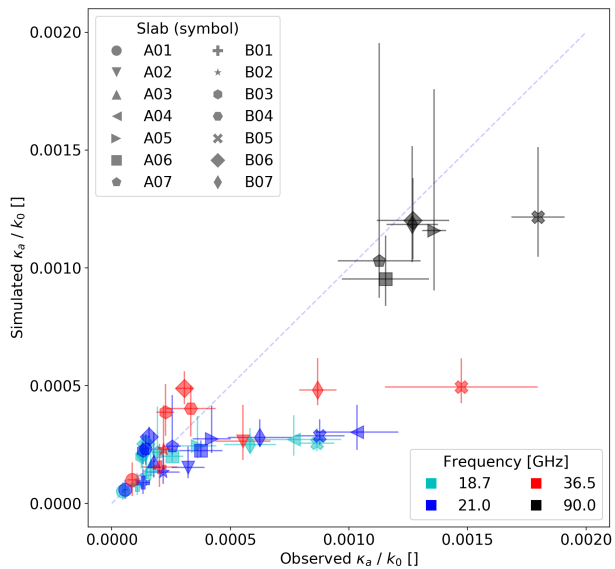


Fig. 7: Scatterplot of ASMEEx subsample absorption coefficient, compared with observed absorption coefficient derived from observations in [27]. Coefficients have been normalized with respect to the wavenumber in free space,  $k_0$ . NB Absorption coefficient is independent of the microstructure model. Observation error bars illustrate the difference between retrievals derived from H- and V-pol observations. Simulation error bars show the range of subsample absorption coefficients relative to the mean.

Errors in ASMEEx  $T_B$  can be explained by  $\kappa_s$  at high  $T_B$  and  $\kappa_a$  at low  $T_B$ . At frequencies of 36.5 GHz and below, scattering coefficients are generally underestimated when compared with the retrieved values, which can explain overestimation of  $T_B$  at high  $T_B$  for the ASMEEx data as there is less simulated scattering of the radiation emitted from the absorber. For low  $T_B$ , where the substrate was a metal plate, differences in  $\kappa_s$  cannot explain the general underestimation in  $T_B$ . Outliers at these low  $T_B$  are generally for slabs A02, A04, B05 and B07, where  $\kappa_a$  and therefore the emission from the snow itself was underestimated. These particular slabs also formed outliers in the central range of ASMEEx  $T_B$ . It is worth noting that slab B05 was considerably thinner (5.4 cm thickness) than other slabs ( $\sim 15$  cm), which may have impacted the accuracy of retrieved  $\kappa_a$  and  $\kappa_s$  for that slab. Less accurate retrievals of  $\kappa_a$  and  $\kappa_s$  can be expected where scattering is low and could partially explain the underestimation of low  $\kappa_s$  in Figure 8.

Vertical structures within snow assumed to be spherically isotropic resulted in higher  $T_B$  errors than for horizontal structures. Whilst ASMEEx slabs were nominally selected for homogeneity within layers, this was not necessarily the case. In addition, analysis of correlation functions in x, y and z directions showed that the slabs were anisotropic (Figure 2). Most of the slabs had an anisotropy factor  $< 1$ , meaning greater correlation lengths in the horizontal than in the vertical. Only

slabs A04, B05 and B07 showed anisotropy factors generally  $> 1$  i.e. larger correlation lengths in the vertical direction more commonly associated with vertical features such as depth hoar chains. Scattering and absorption coefficients and brightness temperature for these slabs were less well simulated than for other slabs.

### C. Simple Snowpack (PAMIR)

Whilst Figure 6b gives an overall picture of  $T_B$  simulations for a shallow refrozen snowpack with simple lower boundary condition, Figure 9 examines the evolution of  $T_B$  over time as the snowpack refreezes. At 4.9 and 10.4 GHz the impact of the snow – and therefore of the microstructure models – is small. There is more variability in the H-pol observations than at V-pol, but the simulations do not capture the observed variability in H-pol  $T_B$ . At higher frequencies the contribution of the snow increases and the impact of the substrate diminishes. Simulations reflect the rapid decline in observed  $T_B$  with increasing depth of refrozen snow at 21 GHz and above although the observed rate at 35 GHz is faster than simulated. For much of the time series, the GRF model demonstrates best agreement with observations. The SHS microstructure model does not show good agreement with observations at 21 and 35 GHz, but is better able to capture the decline in  $T_B$  at 94 GHz for the second refreeze period. The difference in performance between models is shown in the mean error in table II, with TS and GRF demonstrating the lowest errors.

PAMIR is an ideal dataset for exploring reasons for different microstructure model performances as it is relatively small and there are large differences between microstructure models. Figure 10 demonstrates how the correlation functions for different microstructure models, as used in SMRT after averaging, compare with observed correlation functions. Data for the 9th May have been shown as continuous  $T_B$  are available for this day. The dominant horizontal (crust) features evident in sections 2-4 of Figure 3a are reflected by the anisotropy in the real space correlation function in Figure 10, with high correlations in the x-direction tail. Section 5 has vertical features (high correlation in the z-direction tail) whereas section 1 is relatively isotropic. The parametrized correlation functions thus always represent a compromise between the different coordinate directions.

For the real space correlation functions it is possible to compare their performance via naive fit metrics (mean square error) which are shown in Table III. IND microstructure is the least-well fitted microstructure parameter yet  $T_B$  errors in Table II are overall lower than for EXP. However, errors depend on frequency. At 21 GHz, Figure 6b shows higher  $T_B$  errors with IND than EXP, but lower errors at 35 GHz and above. At small scales (e.g.  $r \lesssim 1$  mm), the IND correlation function shown in Figure 10 is higher than EXP and TS real-space microstructure models for sections 2-5, indicating more scattering. At larger scales the lower IND correlation however would suggest less scattering than for other models. In Fourier space, smaller length scales (wavelengths) correspond to larger frequencies. IND could have lower  $T_B$  errors than EXP at higher frequencies because of the poor but higher fit at small scales. IND correlation underestimation at larger scales is more

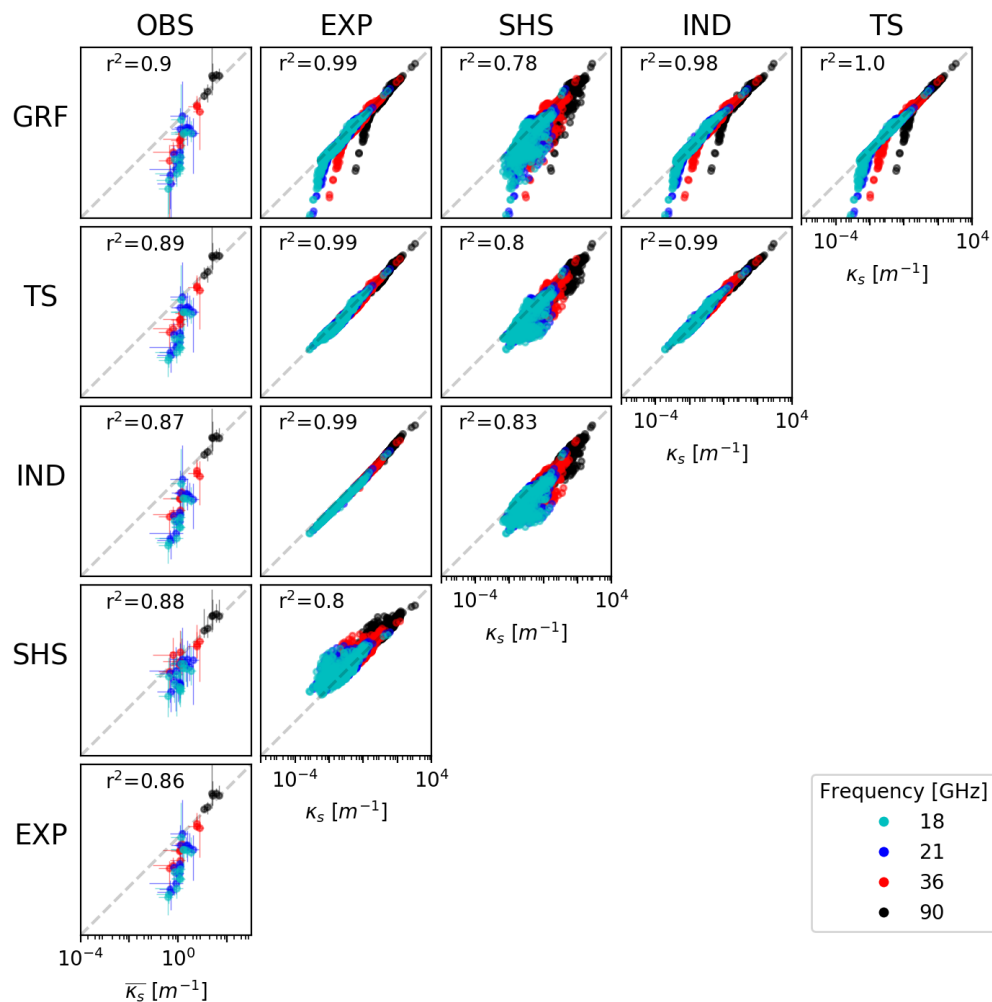


Fig. 8: Scatterplot comparison between scattering coefficients of different microstructure models from ASMEEx subsamples, and a comparison of mean slab scattering coefficients with observed scattering coefficients from [27]. Grey dashed 1:1 line shown. As for Figure 7, observation error bars illustrate the difference between retrievals derived from H- and V-pol observations. Simulation error bars show the range of subsample absorption coefficients relative to the mean.

relevant at lower frequencies, and could explain why  $T_B$  is higher for IND than any other real-space microstructure model at low frequencies.

TS is a better fit to the measured correlation than EXP (although demonstrates EXP-behaviour in the x-direction for sections 2-4). The correlation is also higher than EXP at all scales. The larger TS scattering leads to lower  $T_B$  errors. GRF correlations are generally higher than TS, resulting in further reductions in  $T_B$  errors.

The interpretation of naive mean square fit errors must however taken with caution: In real space the tail of the correlation function dominates the scattering coefficient while absolute values are very small, thus having low influence on the fit error. This also prevents a direct comparison of fit

metrics between real space models and Fourier models (like SHS). For SHS, Fig. 10 however visually reveals that the fit is poor, in particular for low  $k$  values. The difficulties of fitting the SHS sphere model to micro-CT data is well known [14] and remains here a main reason for the poor performance of the SHS model. The comparison reveals that the details of the retrieval of microstructure parameters from CT or thin section image data is a critical, non-trivial problem that extends beyond the scope of this paper. Implications and future work are indicated in the discussion.

#### D. Complex Snowpack (NoSREx)

The NoSREx data provide an opportunity to evaluate SMRT for a deeper, more complex snowpack with soil substrate

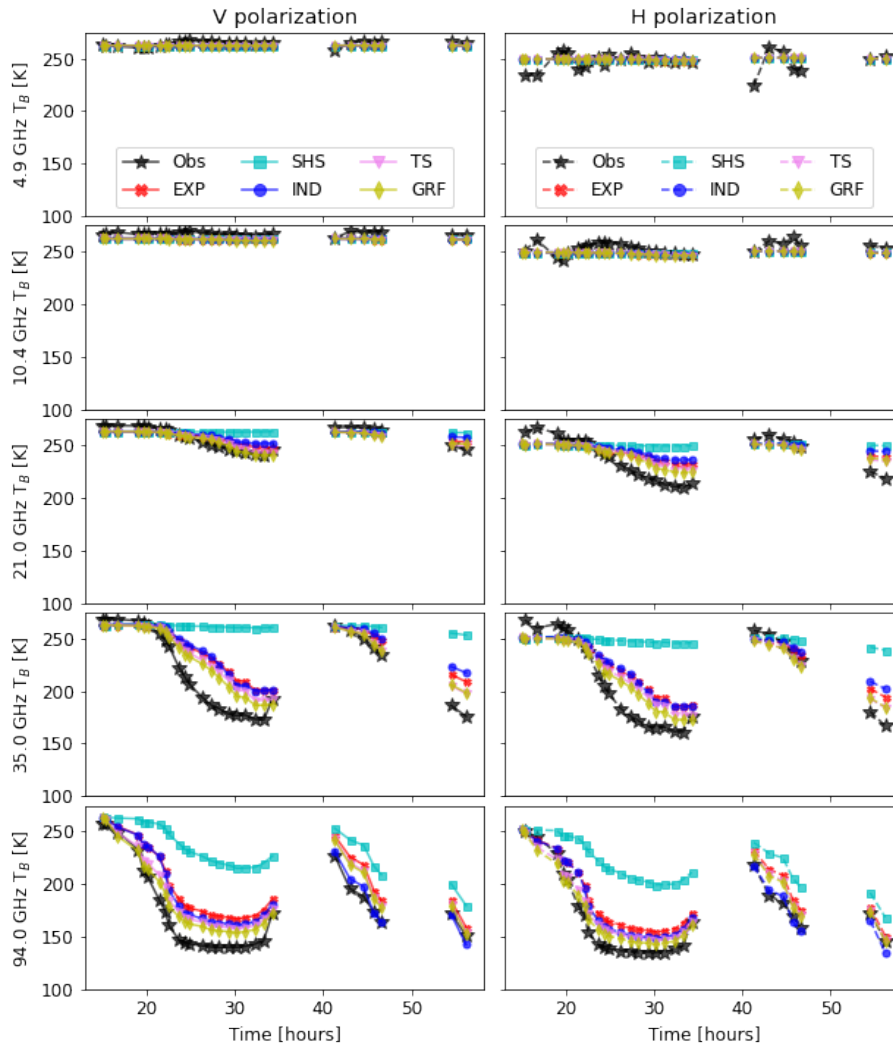


Fig. 9: Time series of brightness temperature for PAMIR experiment (periods with dry surface snow shown)

TABLE III: Real-space fit metrics in x- and z-directions for 9th May PAMIR microstructural parameters, calculated as the sum of the squared residuals of the non-linear fit (*nonlinsq* matlab function) over 100 data points (multiplied by  $10^3$ ). SHS is excluded as it must be fitted in Fourier space and is not comparable.

| Layer   | IND  |     | EXP  |     | TS   |     | GRF  |     |
|---------|------|-----|------|-----|------|-----|------|-----|
|         | x    | z   | x    | z   | x    | z   | x    | z   |
| 1 (top) | 1.6  | 3.5 | 2.2  | 0.3 | 0.6  | 0.3 | 0.6  | 0.3 |
| 2       | 20.2 | 4.6 | 3.9  | 1.7 | 3.9  | 0.6 | 5.0  | 0.7 |
| 3       | 8.5  | 3.6 | 0.4  | 1.8 | 0.4  | 0.1 | 0.6  | 0.2 |
| 4       | 37.1 | 8.6 | 13.1 | 9.5 | 13.1 | 4.3 | 15.1 | 3.9 |
| 5       | 3.6  | 8.5 | 0.8  | 1.6 | 0.3  | 1.6 | 0.4  | 2.1 |

and for a range of incidence angles. Figure 11 shows the angular dependence of  $T_B$  for the EXP, TS and GRF models as these demonstrated the smallest errors in Table II. The difference between simulations for each microstructure model increased with increasing frequency. All three microstructure models agreed well with observations, with RMSE between 3.1 and 4.3 K, and all simulations generally followed the observed shape of the brightness temperature curves. At 21 and 36.5 GHz,  $T_B$  at H-pol were overestimated at incidence angles of  $40^\circ$  and larger.

The polarization difference at 10.65 GHz is too large for all microstructural models, which is an indication that the layer thicknesses could be too thin [34]. Layer thicknesses of 2.37 mm were taken directly from the resolution of the

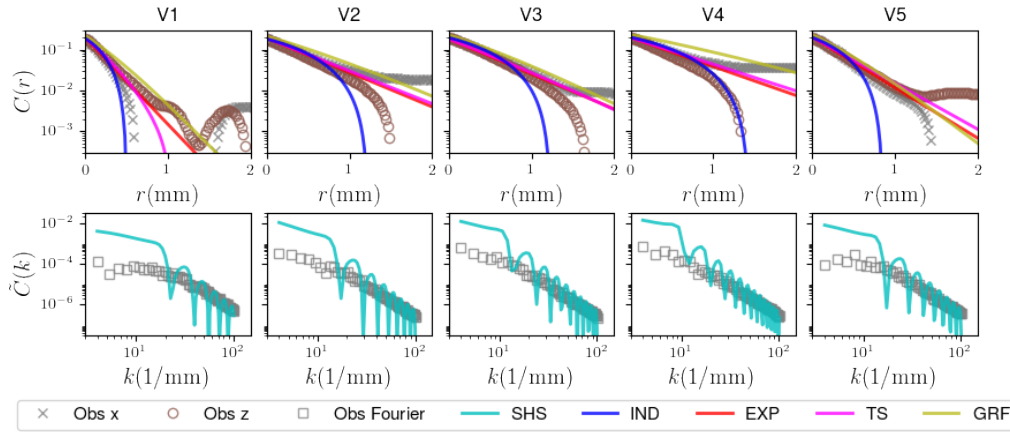


Fig. 10: Comparison between observed and parametrized correlation functions for EXP, IND, TS and GRF in real space (top) and SHS in Fourier space (bottom)

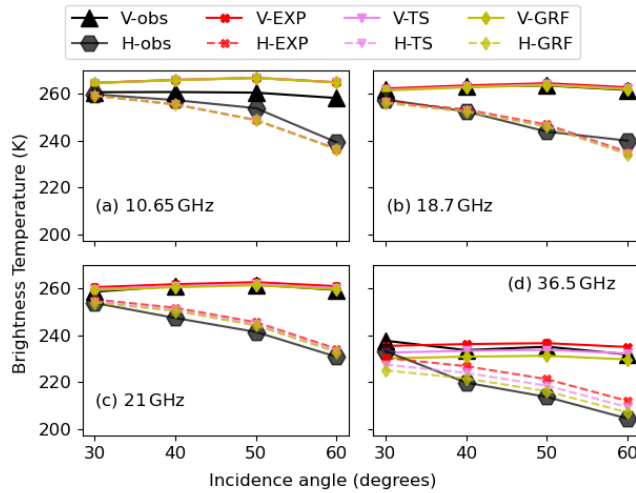


Fig. 11: Brightness temperature variation with incidence angle for NoSREx experiment on 1st March 2012.

micro-CT data, but are actually smaller than the wavelength (28 mm). Resampling of the stratigraphic EXP microstructural properties from 320 to 16 layers of thickness 47.45 mm is illustrated in Figure 12(a) and (b). Resampling captured the trend in density and exponential correlation length, but not the high densities and exponential correlation lengths observed in some thin layers at the base of the snowpack. The effect of lower resolution stratigraphy on simulated  $T_B$  at 10.65 GHz is shown in Figure 12(c). Both H- and V-pol  $T_B$  increased, with a greater impact at H-pol. This narrowed the polarisation difference, but at the cost of  $T_B$  simulation accuracy.

### E. Backscatter

Simulations of total backscatter ( $\sigma_0$ ) with the lower resolution NoSREx snowpack are shown in Figure 13. No observations were made of the bare soil backscatter ( $\sigma_s$ ), so the relative accuracy of the simulations is linked to the chosen

parameterisation of  $\sigma_s = -13$  dB. Consequently no error metrics have been presented and it is not possible to conclude any one microstructure model is a better representation than any other. These simulations are intended to highlight differences (or lack of differences) between microstructure models over a range of incidence angles.

As with the passive simulations, microstructure model differences shown in Figure 13 are greater at higher frequencies.  $\sigma_0$  was highest for the TS model (closely followed by GRF), and lowest for the SHS microstructure model. At 16.7 GHz and incidence angle of  $50^\circ$ ,  $\sigma_0$  for TS microstructure was  $-12.4$  dB, but  $-16.3$  dB for SHS microstructure. Differences between VV and HH  $\sigma_0$  were smaller in the simulations than observations, with a larger decrease in HH  $\sigma_0$  with incidence angle than for VV. At 10.2 and 13.3 GHz observed HH  $\sigma_0$  was higher than VV  $\sigma_0$ , whereas At 16.7 GHz, VV  $\sigma_0$  is higher than HH  $\sigma_0$ . For all simulations VV  $\sigma_0$  is higher than HH  $\sigma_0$ . Cross-polarization simulations have not been presented as SMRT does not currently account for cross-polarization backscatter contribution from the substrate.

Co-polarized backscatter behaviour is broadly captured by SMRT, but the difference between microstructure models can exceed measurement error. No conclusions can be drawn as to the most appropriate microstructure for these data due to uncertainty in the soil backscatter contribution. Improved knowledge of the substrate reflectivity is key to demonstrating simulation accuracy.

## V. DISCUSSION

SMRT accuracy in this study is comparable to or better than other studies, but the main improvement is that it is achieved without *ad hoc* scaling or optimisation of microstructure parameters. The snow parameters are purely based on in-situ measurements. Evaluation of SMRT against these data show largest RMSE for the ASMEEx dataset and smallest for NoSREx. ASMEEx RMSE errors are similar to those found in [18], where mean RMSE in the frequency range 19-89 GHz for both Arctic and Sub-Arctic snow was 16 K and 23 K

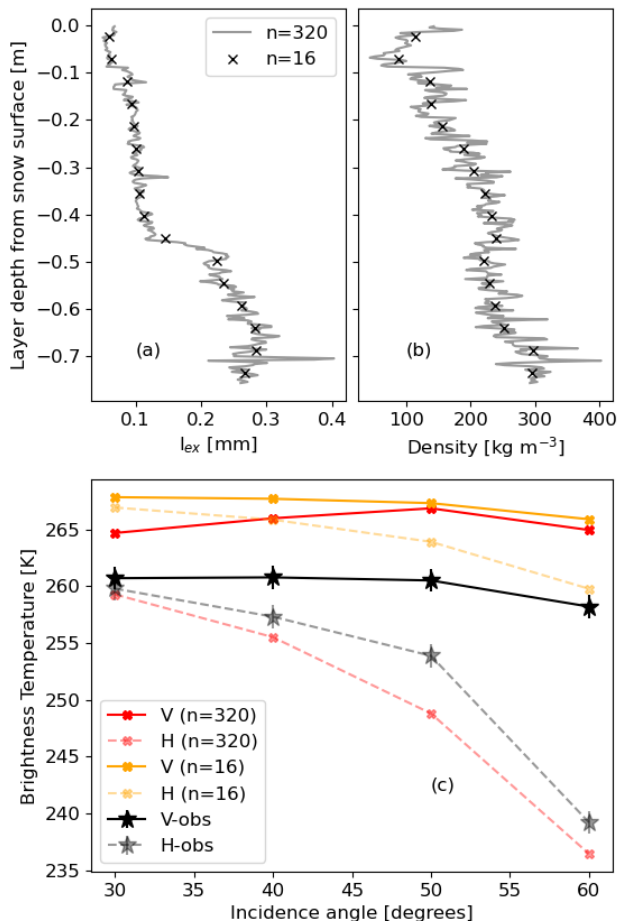


Fig. 12: Impact of changing stratigraphic resolution on 10.65 GHz  $T_B$  curves. High resolution (HR) simulations have 320 layers whereas low resolution (LR) have 16 layers.

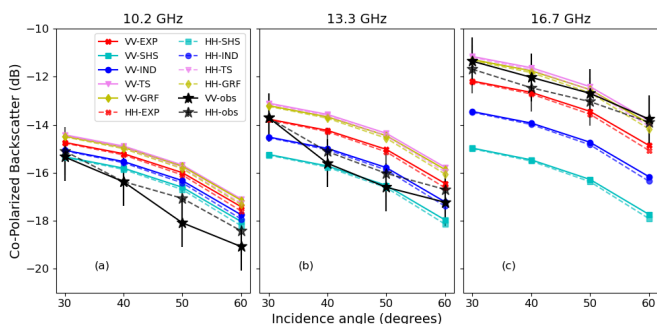


Fig. 13: Comparison between SMRT simulated backscatter and NoSREx observations on 1st March 2012. Panels a, b, c show co-polarized backscatter, whereas panels d, e, f show cross-polarized backscatter. 1 dB measurement error shown

for EXP and SHS microstructure respectively. While RMSE is comparable for ASME<sub>x</sub>, the mean error is lower than in [18]. Studies with other microwave emission models indicate mean RMSE (19-37 GHz) of around 13 K [10] and 16-26 K [12], but as with [18], these were based on microstructure optimisation techniques not applied here. Improvements in SMRT simulations come from the ability to determine and use microstructural parameters directly from micro-CT or thin section images, and from new microstructural models available in SMRT.

Precisely how microstructure parameters are derived requires further attention in a number of areas: (i) fit technique, (ii) anisotropy and (iii) stratigraphy. The current method used to fit the analytical microstructure models to the measured correlation function places no weight on different portions of the curve, meaning fits can be worse at length scales more relevant to particular frequencies.

SHS cannot easily be compared with other microstructure models because the fit to micro-CT data must be done in Fourier space. SHS did not perform well for PAMIR and NoSRE<sub>x</sub>, yet has the potential to perform well as shown by ASME<sub>x</sub>. It is difficult to retrieve parameters for the SHS model [14] as the retrieval tends to identify the lowest possible stickiness as shown in Table I. The fit of the SHS correlation function to experimental data is subject to degeneracy: similar goodness of fits can be obtained by simultaneous variation of diameter and stickiness. For PAMIR, fits to the correlation function at low  $k$  are relatively poor and these parameters are likely more representative at higher frequencies. Microstructure models that have both real-space and Fourier-space analytical correlation functions (IND, EXP, TS) could be used to provide insight into fitting methodology e.g. whether better results can be obtained by fitting in Fourier space. This would also allow to assess whether it is advantageous to perform the orientational averaging of anisotropic snow in real or Fourier space.

Anisotropy has been demonstrated here, even in snow that visually appears homogeneous, and snow with predominantly vertical structures is simulated less well. The simple assumption applied here was that the isotropic parameters currently required in SMRT could be represented by an equally-weighted average of microstructure parameters derived along Cartesian directions. As scattering is non-linearly related to microstructure parameters, this may not be the best approach. Non-equal weight given to the microstructural length scales observed in multiple directions could be explored in the first instance and fitting to the directionally-averaged correlation function could also be tested, although a fundamental advancement in SMRT may be needed to account for anisotropic media properly.

There are greater differences between microstructure models for PAMIR than for ASME<sub>x</sub>, despite similar snow depths and substrate (absorber). This could be a function of greater snow heterogeneity in the PAMIR experiment than for ASME<sub>x</sub>, but more likely because of generally coarser structures (Table I) enhancing the sensitivity to microstructure. PAMIR provides interesting data. In this study ice lenses were not treated as separate thin layers, so there is potential to improve simulations further through explicit consideration of coherence and inter-

layer boundary effects. However, the better performance of TS and GRF compared with other microstructure models within SMRT may mean that the secondary structure parameter is partially able to compensate for coherent and semi-coherent effects.

More generally, we need to rethink how we consider snowpack layers. Snow layers for simulations are often defined by the resolution of the field measurements. Micro-CT allows very fine resolution information, potentially at higher resolution than microwave observations are sensitive to. At 37 GHz the wavelength is 8 mm whereas at 10 GHz it is 30 mm. Since the radiative transfer theory is based on energy transport without tracking the wave phase, specification of thinner layers than the wavelength introduces artificial dielectric discontinuities, which leads to overestimated polarization difference in the simulations [34]. SMRT is equipped with a correction for a sub-wavelength thin layer surrounded by two normal layers, which is relevant for modelling ice lenses, but as with any RT model, SMRT is not able to deal with a snowpack with many layers thinner than the wavelength properly.

PAMIR microstructural parameters were derived from  $\sim 5$  cm sections, which are much larger than the wavelengths of the observations. ASMEEx layers range from 6 mm to 9 mm in thickness: still too fine for the simulations given that the longest wavelength considered is 16 mm. For homogeneous slabs this would not matter, but vertical bars for simulated  $\kappa_s$  in Figure 8 indicate a fair degree of variability in many of the slabs. Agreement with retrieved  $\kappa_s$  depends on whether the slabs conform with the retrieval assumptions, but even good simulations of  $\kappa_s$  can lead to poor  $T_B$  simulations if there are more dielectric discontinuities simulated than observed by the sensors. This does not appear to be a problem for the ASMEEx dataset, but is for NoSREx at 10 GHz where the layers are thinner and a longer wavelength considered. This only concerns H-pol simulations, particularly at large incidence angles.

Larger micro-CT sampling size allows longer tail correlation function analysis but it is not clear whether layers could then become too large in the simulation and neglect dielectric discontinuities observed by the sensor (e.g. single layer snowpack simulations are generally insufficient) so the question is what is the most appropriate resolution for snowpack stratigraphy? Micro-CT should be used to address this question with an added benefit of informing resolution of future field campaigns to minimise micro-CT processing cost.

Some of the above questions could be addressed by using the measured correlation functions directly in SMRT. This is theoretically possible but needs more understanding of how to prevent numerical instabilities caused by the tail of non-decaying correlation functions. Nevertheless, micro-CT offers the potential to look at microstructure in a way that has not been possible previously and offers a pathway to more accurate simulations. However, field sampling is not as easy as for other microstructural observation methods (e.g. SSA and density) and the laboratory processing to extract the 3-D structure is expensive. More work is needed to speed up the micro-CT processing chain and/or develop strategies for relating field measurable quantities to the microstructural model parameters

needed for more accurate simulations.

Accurate quantification of simulation errors is critical for remote sensing applications. For some applications snow may not be the primary focus but affects the measurements so it is necessary to understand the contribution of snow to the observation error budget in e.g. ice thickness retrievals. In numerical weather prediction, atmospheric observation uncertainty due to snow is an essential requirement for assimilation of microwave data in lower troposphere sounding channels. SMRT can also be used in the design of future snow monitoring missions for water supply management.

## VI. CONCLUSION

This paper evaluated SMRT against three field experiments of differing snowpack complexity and covers a range in snow type, snow depth and observation incidence angle. The way snow microstructure is quantified can have a dramatic impact on simulation of microwave brightness temperature or backscatter and becomes increasingly important at higher frequencies. The optimum microstructure model may depend on snow type, and the new two-parameter Teubner-Strey and Gaussian Random Field microstructure models give more accurate brightness temperature simulations than other microstructure models for two of the three field campaigns evaluated.

At present, micro-CT or thin section images are needed to determine the necessary microstructure parameters. Future research should focus on the following: (i) assess methods to fit microstructure models to micro-CT data (ii) how to parameterize microstructure models from field observations, (iii) how to treat snowpack layers given that different frequencies observe different dielectric discontinuities, (iv) how to account for anisotropy in the microstructure, and (v) quantifying simulation uncertainties in support of remote sensing applications. SMRT provides the framework to do this.

## VII. CODE AVAILABILITY

Code and data to run these simulations are available from [https://github.com/smrt-model/smrt\\_evaluation\\_paper](https://github.com/smrt-model/smrt_evaluation_paper)

## ACKNOWLEDGMENT

The authors would like to thank the European Space Agency (ESA) for funding this research (ESTEC:4000112698/14/NL/LvH) and all contributors to SMRT development and testing. Staff at Finnish Meteorological Institute are acknowledged for assisting in data collection for the NoSREx and ASMEEx campaigns. We thank the reviewers for their careful consideration and comments that have helped improve this paper, particularly the suggestion to include microstructure fit metrics.

## REFERENCES

- [1] G. Picard, M. Sandells, and H. Löwe, "SMRT: an activepassive microwave radiative transfer model for snow with multiple microstructure and scattering formulations (v1.0)," *Geoscientific Model Development*, vol. 11, no. 7, pp. 2763–2788, 2018. [Online]. Available: <https://www.geosci-model-dev.net/11/2763/2018/>

- 1  
2  
3  
4  
5  
6  
7  
8  
9  
10  
11  
12  
13  
14  
15  
16  
17  
18  
19  
20  
21  
22  
23  
24  
25  
26  
27  
28  
29  
30  
31  
32  
33  
34  
35  
36  
37  
38  
39  
40  
41  
42  
43  
44  
45  
46  
47  
48  
49  
50  
51  
52  
53  
54  
55  
56  
57  
58  
59  
60
- [2] A. Kontu and J. Pulliainen, "Simulation of Spaceborne Microwave Radiometer Measurements of Snow Cover Using In Situ Data and Brightness Temperature Modeling," *IEEE Transactions on Geoscience and Remote Sensing*, vol. 48, no. 3, pp. 1031–1044, 2010.
- [3] J. Pulliainen, J. Grandell, and M. Hallikainen, "HUT snow emission model and its applicability to snow water equivalent retrieval," *IEEE Transactions on Geoscience and Remote Sensing*, vol. 37, no. 3, pp. 1378–1390, 1999.
- [4] J. Lemmetyinen, J. Pulliainen, A. Rees, A. Kontu, Y. Qiu, and C. Derksen, "Multiple-Layer Adaptation of HUT Snow Emission Model: Comparison With Experimental Data," *IEEE Transactions on Geoscience and Remote Sensing*, vol. 48, no. 7, pp. 2781–2794, 2010.
- [5] C. Mätzler, "Relation between grain-size and correlation length of snow," *Journal of Glaciology*, vol. 48, no. 162, pp. 461–466, Feb. 2002.
- [6] A. Wiesmann and C. Mätzler, "Microwave Emission Model of Layered Snowpacks," *Remote Sensing of Environment*, vol. 70, no. 3, pp. 307–316, Dec. 1999. [Online]. Available: <http://www.sciencedirect.com/science/article/pii/S0034425799000462>
- [7] C. Mätzler and A. Wiesmann, "Extension of the Microwave Emission Model of Layered Snowpacks to Coarse-Grained Snow," *Remote Sensing of Environment*, vol. 70, no. 3, pp. 317–325, Dec. 1999. [Online]. Available: <http://www.sciencedirect.com/science/article/pii/S0034425799000474>
- [8] L. Brucker, G. Picard, L. Arnaud, J.-M. Barnola, M. Schneebeli, H. Brunjail, E. Lefebvre, and M. Fily, "Modeling time series of microwave brightness temperature at Dome C, Antarctica, using vertically resolved snow temperature and microstructure measurements," *Journal of Glaciology*, vol. 57, no. 201, pp. 171–182, Mar. 2011.
- [9] G. Picard, L. Brucker, A. Roy, F. Dupont, M. Fily, A. Royer, and C. Harlow, "Simulation of the microwave emission of multi-layered snowpacks using the Dense Media Radiative transfer theory: the DMRT-ML model," *Geosci. Model Dev.*, vol. 6, no. 4, pp. 1061–1078, Jul. 2013. [Online]. Available: <http://www.geosci-model-dev.net/6/1061/2013/>
- [10] A. Roy, G. Picard, A. Royer, B. Montpetit, F. Dupont, A. Langlois, C. Derksen, and N. Champollion, "Brightness Temperature Simulations of the Canadian Seasonal Snowpack Driven by Measurements of the Snow Specific Surface Area," *IEEE Transactions on Geoscience and Remote Sensing*, vol. 51, no. 9, pp. 4692–4704, 2013.
- [11] N. Rutter, M. Sandells, C. Derksen, P. Toose, A. Royer, B. Montpetit, A. Langlois, J. Lemmetyinen, and J. Pulliainen, "Snow stratigraphic heterogeneity within ground-based passive microwave radiometer footprints: Implications for emission modeling," *Journal of Geophysical Research: Earth Surface*, pp. n/a–n/a, Mar. 2014. [Online]. Available: <http://onlinelibrary.wiley.com/doi/10.1002/2013JF003017/abstract>
- [12] A. Royer, A. Roy, B. Montpetit, O. Saint-Jean-Rondeau, G. Picard, L. Brucker, and A. Langlois, "Comparison of commonly-used microwave radiative transfer models for snow remote sensing," *Remote Sensing of Environment*, vol. 190, pp. 247 – 259, 2017. [Online]. Available: <http://www.sciencedirect.com/science/article/pii/S0034425716304990>
- [13] M. Sandells, R. Essery, N. Rutter, L. Wake, L. Leppänen, and J. Lemmetyinen, "Microstructure representation of snow in coupled snowpack and microwave emission models," *The Cryosphere*, vol. 11, no. 1, pp. 229–246, 2017. [Online]. Available: <https://www.the-cryosphere.net/11/229/2017/>
- [14] H. Löwe and G. Picard, "Microwave scattering coefficient of snow in MEMLS and DMRT-ML revisited: The relevance of sticky hard spheres and tomography-based estimates of stickiness," *The Cryosphere*, vol. 9, no. 6, pp. 2101–2117, 2015.
- [15] M. Durand, E. Kim, and S. Margulis, "Quantifying Uncertainty in Modeling Snow Microwave Radiance for a Mountain Snowpack at the Point-Scale, Including Stratigraphic Effects," *IEEE Transactions on Geoscience and Remote Sensing*, vol. 46, no. 6, pp. 1753–1767, 2008.
- [16] B. Montpetit, A. Royer, A. Langlois, P. Cliche, A. Roy, N. Champollion, G. Picard, F. Domine, and R. Obbard, "New shortwave infrared albedo measurements for snow specific surface area retrieval," *Journal of Glaciology*, vol. 58, no. 211, pp. 941–952, Sep. 2012.
- [17] M. Kerbrat, B. Pinzer, T. Huthwelker, H. W. Gäggeler, M. Ammann, and M. Schneebeli, "Measuring the specific surface area of snow with X-ray tomography and gas adsorption: comparison and implications for surface smoothness," *Atmospheric Chemistry and Physics*, vol. 8, no. 5, pp. 1261–1275, Mar. 2008. [Online]. Available: <http://hal.archives-ouvertes.fr/hal-00296473>
- [18] C. Vargel, A. Royer, O. St-Jean-Rondeau, G. Picard, A. Roy, V. Sasseville, and A. Langlois, "Arctic and subarctic snow microstructure analysis for microwave brightness temperature simulations," *Remote Sensing of Environment*, vol. 242, p. 111754, Jun. 2020. [Online]. Available: <http://www.sciencedirect.com/science/article/pii/S0034425720301243>
- [19] W. Maslanka, L. Leppänen, A. Kontu, M. Sandells, J. Lemmetyinen, M. Schneebeli, M. Proksch, M. Matzl, H.-R. Hannula, and R. Gurney, "Arctic Snow Microstructure Experiment for the development of snow emission modelling," *Geoscientific Instrumentation, Methods and Data Systems*, vol. 5, no. 1, pp. 85–94, 2016. [Online]. Available: <http://www.geosci-instrum-method-data-syst.net/5/85/2016/>
- [20] B. Reber, C. Mätzler, and E. Schanda, "Microwave signatures of snow crusts Modelling and measurements," *International Journal of Remote Sensing*, vol. 8, no. 11, pp. 1649–1665, 1987. [Online]. Available: <http://www.tandfonline.com/doi/abs/10.1080/01431168708954805>
- [21] J. Lemmetyinen, A. Kontu, J. Pulliainen, J. Vehviläinen, K. Rautiainen, A. Wiesmann, C. Mätzler, C. Werner, H. Rott, T. Nagler, M. Schneebeli, M. Proksch, D. Schüttemeyer, M. Kern, and M. Davidson, "Nordic Snow Radar Experiment," *Geoscientific Instrumentation, Methods and Data Systems Discussions*, pp. 1–23, 2016. [Online]. Available: <http://www.geosci-instrum-method-data-syst-discuss.net/gi-2015-29/>
- [22] C. Mätzler, "Improved Born approximation for scattering of radiation in a granular medium," *Journal of Applied Physics*, vol. 83, no. 11, pp. 6111–6117, Jun. 1998. [Online]. Available: <http://scitation.aip.org/content/aip/journal/jap/83/11/10.1063/1.367496>
- [23] A. Sihvola, *Electromagnetic Mixing Formulas and Applications*. London: Institution of Engineering and Technology, Jun. 1999.
- [24] W. Dierking, S. Linow, and W. Rack, "Toward a robust retrieval of snow accumulation over the Antarctic ice sheet using satellite radar," *J. Geophys. Res.*, vol. 117, no. D9, p. D09110, 2012. [Online]. Available: <http://onlinelibrary.wiley.com/doi/10.1029/2011JD017227/abstract>
- [25] L. Tsang, J. Pan, D. Liang, Z. Li, D. Cline, and Y. Tan, "Modeling Active Microwave Remote Sensing of Snow Using Dense Media Radiative Transfer (DMRT) Theory With Multiple-Scattering Effects," *IEEE Transactions on Geoscience and Remote Sensing*, vol. 45, no. 4, pp. 990–1004, 2007.
- [26] M. Teubner, "Level Surfaces of Gaussian Random Fields and Microemulsions," *Europhysics Letters (EPL)*, vol. 14, no. 5, pp. 403–408, Mar. 1991, publisher: IOP Publishing. [Online]. Available: <https://doi.org/10.1209%2F0295-5075%2F14%2F5%2F003>
- [27] W. Maslanka, M. Sandells, R. Gurney, J. Lemmetyinen, L. Leppänen, A. Kontu, M. Matzl, N. Rutter, T. Watts, and R. Kelly, "Derivation and Evaluation of a New Extinction Coefficient for Use With the n-HUT Snow Emission Model," *IEEE Transactions on Geoscience and Remote Sensing*, vol. 57, no. 10, pp. 7406–7417, Oct. 2019.
- [28] W. M. Maslanka, "Extinction of microwave radiation in snow," Ph.D., University of Reading, 2017. [Online]. Available: <http://centaur.reading.ac.uk/72703/>
- [29] S. Leinss, H. Löwe, M. Proksch, and A. Kontu, "Modeling the evolution of the structural anisotropy of snow," *The Cryosphere*, vol. 14, no. 1, pp. 51–75, 2020. [Online]. Available: <https://tc.copernicus.org/articles/14/51/2020/>
- [30] C. Mätzler and A. Wiesmann, "Documentation for MEMLS, Version 3, Microwave Emission Model of Layered Snowpacks," *MEMLS Manual, Version*, vol. 4, p. 12, 2012.
- [31] C. Mätzler, "Applications of the interaction of microwaves with the natural snow cover," *Remote Sensing Reviews*, vol. 2, no. 2, pp. 259–387, 1987. [Online]. Available: <http://www.tandfonline.com/doi/abs/10.1080/02757258709532086>
- [32] U. Wegmüller and C. Mätzler, "Rough bare soil reflectivity model," *IEEE Transactions on Geoscience and Remote Sensing*, vol. 37, no. 3, pp. 1391–1395, 1999.
- [33] M. C. Dobson, F. T. Ulaby, M. T. Hallikainen, and M. A. El-Rayes, "Microwave dielectric behavior of wet soil Part II: Dielectric mixing models," *IEEE Trans. Geosci. Remote Sens.*, vol. 23, no. 1, pp. 35–46, 1985.
- [34] M. Leduc-Leballeur, G. Picard, A. Mialon, L. Arnaud, E. Lefebvre, P. Possenti, and Y. Kerr, "Modeling L-Band Brightness Temperature at Dome C in Antarctica and Comparison With SMOS Observations," *IEEE Transactions on Geoscience and Remote Sensing*, vol. 53, no. 7, pp. 4022–4032, Jul. 2015, conference Name: IEEE Transactions on Geoscience and Remote Sensing.



**Melody Sandells** (she/her) received the M.Sc. degree in physics from Imperial College London, London, U.K., in 1998, and the Ph.D. degree from the University of Reading, Reading, U.K. in 2002. She held postdoctoral research positions at the Centre for Polar Observation and Modelling at University College London and within the National Centre for Earth Observation at the University of Reading. She later became the Director of CORES Science and Engineering Limited, U.K. and was appointed as a Senior Lecturer with the Department of Geography

and Environmental Sciences, Northumbria University, Newcastle upon Tyne, U.K. in 2020. She is President-Elect of the International Commission on Snow and Ice Hydrology. Her research interests include snow and cryosphere physics, earth observation of snow and soil moisture, and soil-snow-vegetation radiative transfer at optical, thermal, and microwave wavelengths.



**Richard Essery** received the B.Sc. degree in mathematical physics from the University of Edinburgh, U.K., in 1987, a certificate of advanced studies in mathematics from the University of Cambridge, U.K., in 1988, and the Ph.D. degree in physics from the University of Cambridge in 1992. He was a member of the land surface processes group at the Met Office Hadley Centre between 1992 and 2002, with responsibility for the representation of surface snow processes in global climate modelling. He took a sabbatical in 1998 with the Canadian National

Hydrological Research Institute. In 2002, he joined the Centre for Glaciology, University of Aberystwyth, as an NERC Advanced Research Fellow, conducting field research in mountain hydrology and micrometeorology in Canada, the United States, Sweden, and Switzerland. He has been at the School of GeoSciences, University of Edinburgh, since 2007 and Professor of Cryosphere-Atmosphere Interactions since 2018. He is also the Secretary General of the International Association of Cryospheric Sciences.



**Henning Löwe** received his diploma degree in physics (1999) and his doctoral degree in theoretical physics (2004) from the University of Göttingen, Germany. His post-doctoral research focused on topics in atmospheric sciences and snow physics. Since 2011, he is a lecturer in the Department of Earth Sciences at ETH, Zurich and since 2018, he is the head of the research group Snow Physics at the WSL Institute for Snow and Avalanche Research SLF in Davos, Switzerland. His work is dedicated to microstructure controls on mechanical, thermal,

electromagnetic and crystal growth processes in snow.



**Nicolas Floury** received the M.Sc. degree in engineering from Télécom Paris Tech, Paris, France, in 1993, and the Ph.D. degree in applied physics from the University Paris Diderot, Paris, France, in 1999. Since then, he has been with the European Space Research and Technology Centre, European Space Agency, Noordwijk, The Netherlands, where he is the Head of the Wave Interaction and Propagation Section. His research interests include signal processing and electromagnetic modeling applied to microwave interaction with natural media.



**Ghislain Picard** received the M.Sc. degree in remote sensing from the University of Paris VII, France in 1997 and the Ph.D. degree from Centre d'Etudes Spatiale de la Biosphere (CESBIO), Toulouse, France, in 2002. During his Ph.D., he developed several electromagnetic models of vegetation backscatter in the microwave range. After postdoctorate research with the Centre for Terrestrial Carbon Dynamics, University of Sheffield, U.K., he joined the Laboratoire de Glaciologie et Géophysique de l'Environnement and Institut des

Geoscience de l'Environnement at Université Grenoble Alpes, France, where he has been working since 2005. His main research is on the Antarctic climate observed through the study of snow using a variety of remote sensing techniques and field experimentation. He is involved in the development of innovative instruments for the characterization of the snow physical properties and of optical and microwave radiative transfer models.



**Anna Kontu** received the M.Sc.(Tech.) degree from Helsinki University of Technology (currently part of Aalto University), Espoo, Finland, in 2006, and the D.Sc.(Tech.) degree from Aalto University, Espoo, Finland, in 2018.

She currently works as Sodankylä Research Infrastructure PI with the Finnish Meteorological Institute's Arctic Space Centre in Sodankylä, Finland. Her research activities focus on microwave remote sensing of seasonal terrestrial snow and soil frost.



**Marie Dumont** received the M.Sc. degree in remote sensing from the Université Paris 6, Paris, France in 2007, and the Ph.D. degree from Paris East University, Paris, France, in 2010. From 2007 to 2010, she conducted her Ph.D. work at the Institut des Geosciences de l'Environnement, Grenoble, where she developed several methods to retrieve snow and ice albedo from remote sensing data. After a postdoctoral research position with Norwegian Polar Institute, Tromsø in 2011, she joined the Centre d'Etudes de la Neige (Centre National de

Recherches Météorologiques), Grenoble, France. Since then, her research has focused on the optical properties of snow, snow detailed modelling and data assimilation.



**Juha Lemmetyinen** received the D.Sc. (Tech) degree in electrical engineering from Aalto University [former Helsinki University of Technology, TKK], Espoo, Finland, in 2012. From 2004 to 2008, he was a Researcher with the TKK Laboratory of Space Technology, Department of Radio Science and Engineering, where he specialized in radiometer calibration techniques and remote sensing. From 2009 to 2013 was a scientist with the Arctic Research Unit, Finnish Meteorological Institute, Helsinki, Finland. Since 2014, he has acted as head of group at FMI

for research on cryosphere processes. His present research interests include applications of microwave radiometers and synthetic aperture radar in remote sensing snow, soil and vegetation, including the development of emission and backscatter models.



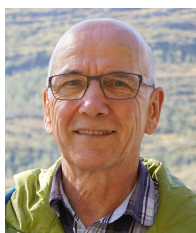
**William Maslanka** received his M.Met degree in Meteorology and PhD in remote sensing and radiative modelling of snow in 2013 and 2017, respectively, from the University of Reading, UK. Between 2017 and 2019, he was a flood modeller and forecaster with the Environment Agency, before returning to the University of Reading as a researcher. His current research interests include microwave remote sensing of surface soil moisture, the applications of drones to remote sensing techniques, and the remote sensing of snow.



**Dr. Samuel Morin** (37) (he/him) is a research scientist with over 10 years experience in the field of snow science. After a PhD in Environmental Sciences completed in 2008, during which he worked on isotopic analyses of atmospheric nitrate in remote areas, he has worked since 2009 at the Snow Research Center (CEN, a research unit of the Centre National de Recherches Météorologiques, CNRM, [www.umr-cnrm.fr](http://www.umr-cnrm.fr), affiliated to Météo-France and CNRS) where he coordinated several research initiatives relevant to the observation and modeling of the mountain snow cover, across various time and space scales. Most recently, he served as Lead Author of the IPCC Special Report on Ocean and Cryosphere in a Changing Climate (SROCC) approved in September 2019.



**Andreas Wiesmann** (M'00-SM'06) received the Diploma degree in physics from the Institute of Applied Physics, University of Bern, Bern, Switzerland, in 1994, and the Ph.D. degree in natural sciences from the University of Bern, Switzerland in 1998. Since 1998, he has been with GAMMA Remote Sensing AG, Gümliigen, Switzerland. His research interests include the interaction of microwaves with natural targets, microwave hardware development, distributed high performance computing, large scale data processing, and computer security.



**Christian Mätzler** was born in 1945 in Kreuzlingen, Switzerland. He studied physics at the University of Bern, with minors in mathematics and geography, M.Sc. in 1970, and Ph.D. in solar radio astronomy in 1974. After postdoctoral research at the NASA Goddard Space Flight Center, Greenbelt, MD, and at the Swiss Federal Institute of Technology (ETH), Zürich, Switzerland, he became Research Group Leader for terrestrial and atmospheric radiometry and remote sensing at the Institute of Applied Physics, University of Bern in 1978. There he received the habilitation in applied physics in 1986 and the title of a Titular Professor in 1992. He spent sabbaticals in 1996 at the Universities of Colorado and Washington and in 2004 at the Paris Observatory. After retirement in July 2010, he started as a consultant for Gamma Remote Sensing. His studies have concentrated on microwave (1100 GHz) signatures for active and passive remote sensing of the atmosphere, snow, ice, soil, and vegetation, as well as on the development of methods for dielectric and propagation measurements for such media. He is Editor of a book on thermal microwave emission with applications in remote sensing. He is interested in physical processes acting at the earth surface and in the atmosphere.